Meshless analysis of potential problems in three dimensions with the hybrid boundary node method

Jianming Zhang*,†, Masataka Tanaka and Toshiro Matsumoto

Faculty of Engineering, Shinshu University, Nagano 380-8553, Japan

SUMMARY

Combining a modified functional with the moving least-squares (MLS) approximation, the hybrid boundary node method (Hybrid BNM) is a truly meshless, boundary-only method. The method may have advantages from the meshless local boundary integral equation (MLBIE) method and also the boundary node method (BNM). In fact, the Hybrid BNN requires only the discrete nodes located on the surface of the domain.

   The Hybrid BNM has been applied to solve 2D potential problems. In this paper, the Hybrid BNM is extended to solve potential problems in three dimensions. Formulations of the Hybrid BNM for 3D potential problems and the MLS approximation on a generic surface are developed. A general computer code of the Hybrid BNM is implemented in C++. The main drawback of the 'boundary layer effect' in the Hybrid BNM in the 2D case is circumvented by an adaptive face integration scheme. The parameters that influence the performance of this method are studied through three different geometries and known analytical fields. Numerical results for the solution of the 3D Laplace's equation show that high convergence rates with mesh refinement and high accuracy are achievable. Copyright © 2004 John Wiley & Sons, Ltd.

KEY WORDS: meshless methods; hybrid boundary node method; moving least-squares approximation

1. INTRODUCTION

In recent years, the meshless methods have gained popularity very quickly ever since the publication of the diffuse element method [1] and the element free Galerkin method (EFG) [2]. This is because the mesh-based methods, such as FEM and BEM, have much difficulty in solving problems involving changing domains such as large deformation or crack propagation; and the task of mesh generation of a 3D object with complicated geometry is often arduous, time-consuming and error prone. Many kinds of meshless method have been proposed so far [3–6]. These methods can be simply sorted into two categories: the domain type and the

---

Copyright © 2004 John Wiley & Sons, Ltd.

boundary type. The domain type meshless method is represented by the element free Galerkin method which uses a global symmetric weak form and the shape functions from the moving least-squares (MLS) approximation. However, although no mesh is required in the EFG method for the variable interpolation, background cells are inevitable for the 'energy' integration.

To get rid of the background cells and hence achieve a truly meshless method, Atluri and his co-workers have developed two meshless methods of domain type: the meshless local boundary integral equation [7] (MLBIE) and the meshless local Petrov–Galerkin (MLPG) approach [8]. Both methods use local weak forms over a local sub-domain and shape functions from the MLS approximation, and are truly meshless, because no 'finite element or boundary element mesh' is required either for the variable interpolation or for the 'energy' integration. All integrals can be easily evaluated over regularly shaped domains (for example, circles in 2D problems and spheres in 3D problems) and their boundaries.

In order to retain both the meshless attribute of the MLS approximation and the dimensionality advantage of the BEM, Mukherjee *et al.* introduced the MLS interpolants into the Boundary Integral Equations (BIE) and produced a boundary type meshless method, which they call the boundary node method (BNM) [9]. This method only requires a nodal data structure on the bounding surface of a body whose dimension is less by one than that of the domain itself; however, this method is not a truly meshless one, as an underlying cell structure is again used for numerical integration.

A question arises here—does there possibly exist a method of solving boundary value problems that only requires nodes constructed on the surface of the domain and does not require any cells either for interpolation of the solution variables or for the numerical integration? If such a method exists, it will simplify the input data structure greatly, and will be an important step in the direction towards complete analysis automation.

The answer is positive. One of the candidates is the Hybrid Boundary Node Method [10] (Hybrid BNM), proposed by Zhang *et al.*, which combines the MLS interpolation scheme with the hybrid displacement variational formulation. Nevertheless, the Hybrid BNM has a drawback of serious 'boundary layer effect', i.e. the accuracy of results in the vicinity of the boundary is very sensitive to the proximity of the interior points to the boundary. To avoid this hindrance, they further proposed the Regular Hybrid Boundary Node Method [11–13] (RHBNM). In contrast to other hybrid boundary element models, the fundamental solutions are used in the RHBNM with their source points located outside the domain other than on the boundary. Numerical computations show that results from the RHBNM are no more sensitive to the proximity of the interior points to the boundary and very high accuracy can be achieved with a small number of boundary nodes. However, the outside arrangement of the source points of the fundamental solution also causes a series of new problems. For instance, it will be difficult to find a proper place to put the source points when a concave boundary is considered. Another drawback of the RHBNM is that the accuracy of results depends on the distance of the source point to the boundary. Usually, the far the distance is, the more accurate the results will be; while, unfortunately, too far distance may also result in an ill-conditioned matrix and lead to numerical instability. Therefore, it would be more advantageous to overcome the 'boundary layer effect' with the source points of fundamental solution located on the boundary other than outside the domain.

The hybrid boundary element method was first proposed by Schnack [14], in which he stressed using the boundary element method to generate a hybrid stress finite element model which gives rapid convergence of the results and accurate solutions for stress concentration

problems. Dumont [15] has presented a hybrid stress boundary element formulation based on Hellinger–Reissner principle with stresses in the domain and displacements on the boundary as independent functions. DeFiguredo and Brebbia [16] have introduced a hybrid displacement variational formulation of BEM, which is based on a modified functional using three independent variables, i.e. displacements and tractions on the boundary and displacements inside the domain. This approach uses the classical fundamental solution to interpolate the displacements in the domain and thus allows for the transfer of the domain integrals to the boundary. The resulting system of equations is written in terms of the boundary displacements only, and has the advantage of being symmetrical, which is easy to couple with the FEM.

In this paper, the purpose of using the modified functional is to obtain a truly meshless boundary-only method by combining it with the MLS approximation, other than to obtain the symmetrical system of equations. The variables inside the domain are interpolated by the fundamental solutions while the boundary unknowns are approximated by the MLS approximation scheme. By localizing the integration domain to a regular sub-domain, a truly meshless Hybrid BNM for solving 3D potential problems is achieved. Formulations of the MLS approximation on a generic surface are developed. In order to overcome the 'boundary layer effect', an adaptive face integration scheme is proposed. Several numerical examples are also presented to show the efficiency of the present method.

In Section 2, the MLS approximation on a generic 3D surface is described briefly. Formulations of the Hybrid BNM for 3D potential problems are developed in Section 3. The recovery of the secondary results and the adaptive face integration scheme are demonstrated in Section 4. Numerical examples for 3D potential problems are given in Section 5. The paper ends with conclusions in Section 6.

2. THE MLS APPROXIMATION SCHEME ON A GENERIC 3D SURFACE

An MLS interpolation scheme on a generic surface is proposed here. Since the nodes lie on the boundary $\partial\Omega$ of a 3D body Ω in the Hybrid BNM, the MLS approximation is only needed on the bounding surfaces. It is assumed that, for 3D problems, the bounding surface $\partial\Omega$ of a 3D body is the union of piecewise smooth segments called panels. The MLS interpolation is performed independently on each panel, respectively, so that the discontinuity at edges and corners is avoided.

The first step for MLS interpolation on a generic surface is to choose a proper co-ordinate system. In CAD software, surfaces are usually represented in parametric forms

$$x = x_1(s_1, s_2), \quad x_2 = x_2(s_1, s_2), \quad x_3 = x_3(s_1, s_2) \tag{1}$$

where the parametric co-ordinates are defined in the range, $s_1, s_2 \in [0, 1]$. To make the data structure of the geometry consistent with CAD software, and to render a MLS scheme in general sense for all kinds of surface, the MLS interpolation on a surface in this study is performed in the parametric plane as well. To this end and for problems in potential theory, the unknown potential function and its normal gradient on a surface are also expressed in the

parametric forms as

$$
\left.\begin{aligned}
u(x_1, x_2, x_3) &= u(x_1(s_1, s_2), x_2(s_1, s_2), x_3(s_1, s_2)) = u(s_1, s_2) \\
q(x_1, x_2, x_3) &\equiv \frac{\partial u}{\partial n} = q(x_1(s_1, s_2), x_2(s_1, s_2), x_3(s_1, s_2)) = q(s_1, s_2)
\end{aligned}\right\} \tag{2}
$$

where n is a unit outward normal to $\partial\Omega$ at the point (x_1, x_2, x_3) on the surface.

The MLS interpolation scheme will be coupled later with a 3D hybrid 'displacement' variational formulation which uses three independent variables, i.e. potential and normal flux on the boundary and potential inside the domain. In view of the fact that the potential and normal flux on the 2D bounding surface will be interpolated by the MLS scheme, only the $\tilde{u}$ and $\tilde{q}$ defined as the boundary potential and normal flux will be addressed in this section.

For a panel over which a number of randomly located nodes $\{s^I\}$, $I = 1, 2, \ldots, N$, the MLS interpolants for $\tilde{u}$ and $\tilde{q}$ are defined by

$$
\tilde{u}(s) = \sum_{j=1}^{m} p_j(s) a_j(s) = \mathbf{p}^{\mathbf{T}}(s)\mathbf{a}(s) \tag{3}
$$

and

$$
\tilde{q}(s) = \sum_{j=1}^{m} p_j(s) b_j(s) = \mathbf{p}^{\mathbf{T}}(s)\mathbf{b}(s) \tag{4}
$$

where $\mathbf{s}$ is a generic point with parametric co-ordinates (s_1, s_2), $p_1 = 1$ and $p_j(s)$, $j = 2, \ldots, m$ are monomials in (s_1, s_2). The monomials $p_j(s)$ provide the intrinsic polynomial bases for $\tilde{u}$ and $\tilde{q}$. In the numerical implementation presented later in this study, a quadratic background basis is used, i.e.

$$
\mathbf{p}^{\mathbf{T}}(s) = [1, s_1, s_2, s_1^2, s_1 s_2, s_2^2], \quad m = 6 \tag{5}
$$

The coefficient vectors $\mathbf{a}(s)$ and $\mathbf{b}(s)$ are determined by minimizing weighted discrete L_2 norms, defined as

$$
J_1(s) = \sum_{I=1}^{N} w_I(s) \left[\mathbf{p}^{\mathbf{T}}(s^I)\mathbf{a}(s) - \hat{u}_I \right]^2 \tag{6}
$$

$$
J_2(s) = \sum_{I=1}^{N} w_I(s) \left[\mathbf{p}^{\mathbf{T}}(s^I)\mathbf{b}(s) - \hat{q}_I \right]^2 \tag{7}
$$

where points $\mathbf{s}^I$ are boundary nodes, $\mathbf{s}$ is an evaluation point on the panel, N is the number of the boundary nodes in the neighbourhood of $\mathbf{s}$ for which the weight functions $w_I(s) > 0$. It should be noted here that $\hat{u}_I$ and $\hat{q}_I$, $I = 1, 2, \ldots, N$ are simply parameters other than the nodal values of the unknowns $\tilde{u}_I$ and $\tilde{q}_I$ in general. This distinction between $\hat{u}_I$ and $\tilde{u}_I$ (or $\hat{q}_I$ and $\tilde{q}_I$) is very important because MLS interpolants do not have the delta function property.

Solving for $\mathbf{a}(s)$ and $\mathbf{b}(s)$ by minimizing J_1 and J_2 in Equations (6) and (7), and substituting them into Equations (3) and (4) gives a relation which can be written in the forms with

interpolation functions similar to those used in FEM, as follows:

$$\tilde{u}(\mathbf{s}) = \sum_{I=1}^{N} \Phi_I(\mathbf{s})\hat{u}_I \tag{8}$$

$$\tilde{q}(\mathbf{s}) = \sum_{I=1}^{N} \Phi_I(\mathbf{s})\hat{q}_I \tag{9}$$

where

$$\Phi_I(\mathbf{s}) = \sum_{j=1}^{m} p_j(\mathbf{s}) \left[A^{-1}(\mathbf{s}) B(\mathbf{s}) \right]_{jI} \tag{10}$$

with matrices $A(\mathbf{s})$ and $B(\mathbf{s})$ defined by

$$A(\mathbf{s}) = \sum_{I=1}^{N} w_I(\mathbf{s})\mathbf{p}(\mathbf{s}^I)\mathbf{p}^{\mathbf{T}}(\mathbf{s}^I) \tag{11}$$

and

$$B(\mathbf{s}) = \left[w_1(\mathbf{s})\mathbf{p}(\mathbf{s}^1), \, w_2(\mathbf{s})\mathbf{p}(\mathbf{s}^2), \ldots, w_N(\mathbf{s})\mathbf{p}(\mathbf{s}^N) \right] \tag{12}$$

The MLS approximation is well-defined only when the matrix A in Equation (11) is non-singular.

The $\Phi_I(\mathbf{s})$ is usually called the shape function of the MLS approximation corresponding to the nodal point $\mathbf{s}^I$. From Equations (10) and (12), it is seen that $\Phi_I(\mathbf{s}) = 0$ when $w_I(\mathbf{s}) = 0$. The fact that $\Phi_I(\mathbf{s})$ vanishes for $\mathbf{s}$ not in the support of nodal point $\mathbf{s}^I$ preserves the local character of the MLS approximation.

The partial derivatives of $\Phi_I(\mathbf{s})$ are obtained as in Reference [2] to be

$$\Phi_{I,k} = \sum_{j=1}^{m} [p_{j,k}(A^{-1}B)_{jI} + p_j(A^{-1}B_{,k} + A^{-1}_{,k}B)_{jI}] \tag{13}$$

in which $A^{-1}_{,k} = (A^{-1})_{,k}$ represents the derivative of the inverse of A with respect to s_k, $k = 1, 2$, given by

$$A^{-1}_{,k} = - A^{-1}A_{,k}A^{-1} \tag{14}$$

where, $(\ )_{,k}$ denotes $\partial(\ )/\partial s_k$.

In implementing the MLS approximation, the weight functions should be chosen at first. Several kinds of weight functions can be found in the literatures; the choice of weight functions and the consequences of a choice in EFG method are discussed in detail elsewhere [3]. In this study, we use the Gaussian weight function. The Gaussian weight function corresponding to a node $\mathbf{s}^I$ can be written by

$$w_I(\mathbf{s}) = \begin{cases} \dfrac{\exp[-(d_I/c_I)^2] - \exp[-(\hat{d}_I/c_I)^2]}{1 - \exp[-(\hat{d}_I/c_I)^2]}, & 0 \leqslant d_I \leqslant \hat{d}_I \\ 0, & d_I \geqslant \hat{d}_I \end{cases} \tag{15}$$

where c_I is a constant controlling the shape of the weight function, and $\hat{d}_I$ is the size of the support for the weight function w_I. It can be seen from the above equation that the weight function has a compact support determined by the parameter $\hat{d}_I$. The compact support is also an associated range of influence of each node. In the past, the shape of the compact support is usually chosen to be circle in meshless literatures, while in this study, we choose ellipse for the shape of the compact support with $\hat{d}_I$ being the half-length of major axis of the ellipse. Denoting the half-length of minor axis by $\hat{d}_I'$, we have the following expression for d_I:

$$d_I = \sqrt{(s_1 - s_1^I)^2 + \frac{\hat{d}_I^2}{\hat{d}_I'^2}(s_2 - s_2^I)^2}$$

In order to ensure the regularity of A, the $\hat{d}_I$ and $\hat{d}_I'$ should be chosen in such a way that they are large enough to have a sufficient number of nodes which are covered in the domain of definition of every sample point ($N \geqslant m$). But too large $\hat{d}_I$ and $\hat{d}_I'$ will lose the local character of the MLS interpolation, or even lead to an ill-conditioned matrix A. In this study, $\hat{d}_I$ and $\hat{d}_I'$ are chosen such that $4m$–$8m$ nodes are included in the support of a node.

3. DEVELOPMENT OF THE HYBRID BOUNDARY NODE METHOD

The potential problem in three dimensions governed by Laplace's equation with boundary conditions is written as

$$u_{,ii} = 0 \quad \forall x \in \Omega$$
$$u = \bar{u} \quad \forall x \in \Gamma_u \qquad (16)$$
$$u_{,i} n_i \equiv q = \bar{q} \quad \forall x \in \Gamma_q$$

where the domain Ω is enclosed by $\Gamma = \Gamma_u + \Gamma_q$; $\bar{u}$ and $\bar{q}$ are the prescribed potential and the normal flux, respectively, on the essential boundary Γ_u and on the flux boundary Γ_q; and n is the outward normal direction to the boundary Γ, with components n_i, $i = 1, 2, 3$.

The hybrid boundary node method proposed in this paper is based on a modified variational principle. The functions assumed to be independent are:

- potential field in the domain, u;
- boundary potential field, $\tilde{u}$;
- boundary normal flux, $\tilde{q}$.

The corresponding variational functional Π_{AB} is defined as follows:

$$\Pi_{AB} = \int_\Omega \tfrac{1}{2} u_{,i} u_{,i} \, d\Omega - \int_\Gamma \tilde{q}(u - \tilde{u}) \, d\Gamma - \int_{\Gamma_q} \bar{q}\tilde{u} \, d\Gamma \qquad (17)$$

where, the boundary potential $\tilde{u}$ satisfies the essential boundary condition, i.e. $\tilde{u} = \bar{u}$ on Γ_u.

The variation of Π_{AB} becomes

$$\delta\Pi_{AB} = \int_\Gamma (q - \tilde{q})\delta u \, \mathrm{d}\Gamma - \int_\Omega u_{,ii}\delta u \, \mathrm{d}\Omega + \int_{\Gamma_q} (\tilde{q} - \bar{q})\delta\tilde{u} \, \mathrm{d}\Gamma - \int_\Gamma (u - \tilde{u})\delta\tilde{q} \, \mathrm{d}\Gamma \qquad (18)$$

where $q = \partial u/\partial n$.

The vanishing of $\delta\Pi_{AB}$ for arbitrary variations δu in Ω, $\partial\tilde{u}$ and $\delta\tilde{q}$ on Γ, with $\delta\tilde{u} = 0$ on Γ_u, gives the following Euler equations:

$$
\begin{aligned}
u_{,ii} &= 0 \quad \text{in } \Omega \\
u - \tilde{u} &= 0 \quad \text{at } \Gamma \\
q - \tilde{q} &= 0 \quad \text{at } \Gamma \\
\tilde{q} - \bar{q} &= 0 \quad \text{at } \Gamma_q
\end{aligned}
\qquad (19)
$$

Consequently the solution of the problem is now given in terms of the functions u, $\tilde{u}$ and $\tilde{q}$, which makes $\delta\Pi_{AB}$ stationary.

With the vanishing of $\delta\Pi_{AB}$, we also have the following equivalent integral equations:

$$\int_\Gamma (q - \tilde{q})\delta u \, \mathrm{d}\Gamma - \int_\Omega u_{,ii}\delta u \, \mathrm{d}\Omega = 0 \qquad (20)$$

$$\int_\Gamma (u - \tilde{u})\delta\tilde{q} \, \mathrm{d}\Gamma = 0 \qquad (21)$$

$$\int_{\Gamma_q} (\tilde{q} - \bar{q})\delta\tilde{u} \, \mathrm{d}\Gamma = 0 \qquad (22)$$

If we impose the flux boundary condition, $\tilde{q} = \bar{q}$, just in the same way as the essential boundary condition after the matrices have been computed, Equation (22) holds. So it can be omitted temporarily in the following development.

Equations (20) and (21) hold for any portion of the domain Ω, for example a sub-domain Ω_s and its boundary Γ_s and L_s (see Figure 1). Following the procedure in Reference [17], we use the following weak forms for the sub-domain Ω_s and its boundary Γ_s and L_s to replace Equations (20) and (21):

$$\int_{\Gamma_s + L_s} (q - \tilde{q}_s)v \, \mathrm{d}\Gamma - \int_{\Omega_s} u_{,ii}v \, \mathrm{d}\Omega = 0 \qquad (23)$$

$$\int_{\Gamma_s + L_s} (u - \tilde{u}_s)v \, \mathrm{d}\Gamma = 0 \qquad (24)$$

where v is a weight function; $\tilde{u}_s$ and $\tilde{q}_s$ are the boundary potential and normal flux at the boundary $\partial\Omega_s$, respectively. It should be noted further that the above equations hold irrespective of the size and the shape of Ω_s and its boundary $\partial\Omega_s$. This is an important observation which forms the basis of the present formulation. We now deliberately choose a simple regular shape for Ω_s. The most regular shape of a sub-domain is an n-dimensional sphere for a
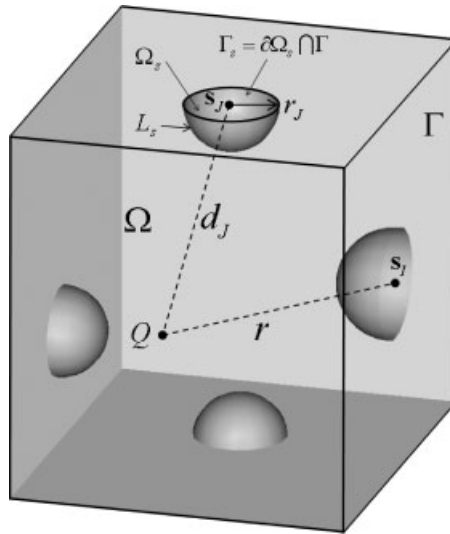
Figure 1. The local domain centred at a node $\mathbf{s}_J$ and the source point of fundamental
solution corresponding to a node $\mathbf{s}_I$.

boundary value problem defined in an *n*-dimensional space. In the present paper, we choose
Ω_s as the intersection of the domain Ω and a sphere centred at a boundary node $\mathbf{s}_J$ (see
Figure 1).

In Equations (23) and (24), $\tilde{u}_s$ and $\tilde{q}$ on Γ_s can be represented by $\tilde{u}$ and $\tilde{q}$ expressed in
Equations (8) and (9) since Γ_s is a portion of Γ, but $\tilde{u}_s$ and $\tilde{q}_s$ on L_s has not been defined
yet. To solve this problem, we select v such that all integrals over L_s vanish. This can be
easily accomplished by using the weight function in the MLS approximation for v, with the
half-length of the major axis $\hat{d}_I$ of the support of the weight function being replaced by the
radius r_J of the sub-domain Ω_s, i.e.

$$v_J(Q) = \begin{cases} \dfrac{\exp[-(d_J/c_J)^2] - \exp[-(r_J/c_J)^2]}{1 - \exp[-(r_J/c_J)^2]}, & 0 \leqslant d_J \leqslant r_J \\ 0, & d_J \geqslant r_J \end{cases} \tag{25}$$

where d_J is the distance between a point Q, in the domain Ω, and the nodal point $\mathbf{s}_J$. Therefore,
v vanishes on L_s, and Equations (23) and (24) can be rewritten as

$$\int_{\Gamma_s} (q - \tilde{q})v \, d\Gamma - \int_{\Omega_s} u_{,ii} v \, d\Omega = 0 \tag{26}$$

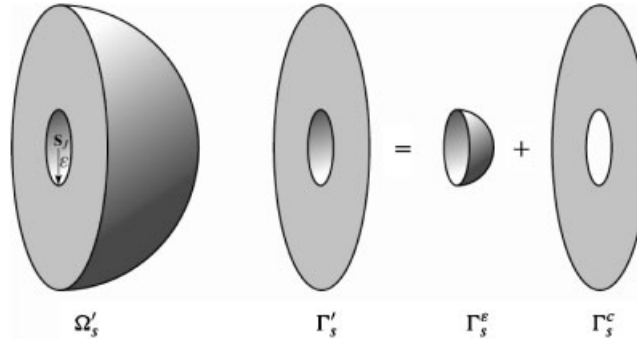$$\int_{\Gamma_s} (u - \tilde{u})v \, d\Gamma = 0 \tag{27}$$

Figure 2. Separation of sub-surfaces during sub-domain modification.

Further, the u inside the domain is approximated by

$$u = \sum_{I=1}^{NN} U_I x_I \tag{28}$$

and hence

$$q = \sum_{I=1}^{NN} \frac{\partial U_I}{\partial n} x_I \tag{29}$$

where U_I is the fundamental solution with the source at a node $\mathbf{s}_I$; x_I are unknown parameters; NN is the total number of boundary nodes.

For 3D potential problems, the fundamental solution is

$$U_I = \frac{1}{4\pi} \frac{1}{r(Q, s_I)} \tag{30}$$

where Q and $\mathbf{s}_I$ are the field point and the source point respectively.

The approximation formulae of Equations (28) and (29) lead to singularities in integral equations (26) and (27) when node $\mathbf{s}_J$ and node $\mathbf{s}_I$ are coincident. The arising singularity in Equation (27), however, is weak and can be evaluated directly. Special treatment is required for Equation (26) in which the singularity is strong. By modifying the sub-domain Ω_s as shown in Figure 2, such that a small sphere of radius ε, centred at node $\mathbf{s}_J$ where singularity occurs, is subtracted from it, the new sub-domain Ω_s' with boundary $L_s \cup \Gamma_s^\varepsilon \cup \Gamma_s^c$ is thus introduced. Excluding node $\mathbf{s}_J$ from the considered sub-domain results in vanishing of the domain integral in Equation (26) in the limit $\Omega_s' \to \Omega_s$, i.e.

$$\lim_{\varepsilon \to 0} \int_{\Omega_s'} u_{,ii} v \, \mathrm{d}\Omega = 0 \tag{31}$$

Equation (26) can then be rewritten as

$$\lim_{\varepsilon \to 0} \int_{\Gamma_s^\varepsilon} q v \, \mathrm{d}\Gamma + \lim_{\varepsilon \to 0} \int_{\Gamma_s^c} q v \, \mathrm{d}\Gamma - \lim_{\varepsilon \to 0} \int_{\Gamma_s^c} \tilde{q} v \, \mathrm{d}\Gamma = 0 \tag{32}$$

In the above equation, the first term is non-zero only if node $\mathbf{s}_J$ coincides with node $\mathbf{s}_I$; at the same time, the second term is a singular integral in Cauchy Principal Value sense. All these singular integrals, along with the first term, contribute only to the main diagonal elements of the coefficient matrix. Since these strongly singular integrals can be calculated by applying a special solution (e.g. a uniform field), the direct numerical evaluation of them is avoided. Therefore, for the sake of simplicity only, we will use instead of Equation (32) the following expression:

$$\int_{\Gamma_s} q v \, \mathrm{d}\Gamma - \int_{\Gamma_s} \tilde{q} v \, \mathrm{d}\Gamma = 0 \tag{33}$$

By substituting Equations (8), (9), (25), (28) and (29) into Equations (33) and (27), we have

$$\sum_{I=1}^n \int_{\Gamma_s} \frac{\partial U_I}{\partial n} v_J(Q) x_I \, \mathrm{d}\Gamma = \sum_{I=1}^n \int_{\Gamma_s} \Phi_I(\mathbf{s}) v_J(Q) \hat{q}_I \, \mathrm{d}\Gamma$$

$$\sum_{I=1}^n \int_{\Gamma_s} U_I v_J(Q) x_I \, \mathrm{d}\Gamma = \sum_{I=1}^n \int_{\Gamma_s} \Phi_I(\mathbf{s}) v_J(Q) \hat{u}_I \, \mathrm{d}\Gamma \tag{34}$$

In the present formulation, the proper choice of the local boundary regions Γ_s is of crucial importance for 3D problems. The theoretically ideal Γ_s are chosen in such a way that they cover the whole boundary of the body and do not overlap each other. Unfortunately, this condition can not be fulfilled in the 3D case. However, our computations in the 2D case indicate that the present formulation can give acceptable results whether the local regions Γ_s overlap each other, or the union of all local regions Γ_s does not cover the whole boundary [10]. In this paper, we use ellipse in the parametric plane as the shape of the local regions Γ_s and investigate the optimal size of Γ_s.

Using the above equations for all nodes, we obtain the following system of equations:

$$\mathbf{U}\mathbf{x} = \mathbf{H}\hat{\mathbf{q}} \tag{35}$$

$$\mathbf{V}\mathbf{x} = \mathbf{H}\hat{\mathbf{u}} \tag{36}$$

where

$$U_{IJ} = \int_{\Gamma_s^J} \frac{\partial U_I}{\partial n} v_J(Q) \, \mathrm{d}\Gamma$$

$$V_{IJ} = \int_{\Gamma_s^J} U_I v_J(Q) \, \mathrm{d}\Gamma$$

$$H_{IJ} = \int_{\Gamma_s^J} \Phi_I(\mathbf{s}) v_J(Q) \, \mathrm{d}\Gamma$$

$$\mathbf{x}^\mathbf{T} = [x_1, x_2, \ldots, x_n]$$

$$\hat{\mathbf{q}}^\mathbf{T} = [\hat{q}_1, \hat{q}_2, \ldots, \hat{q}_n]$$

$$\hat{\mathbf{u}}^\mathbf{T} = [\hat{u}_1, \hat{u}_2, \ldots, \hat{u}_n]$$

From Equation (31) we have

$$\mathbf{x} = \mathbf{V}^{-1}\mathbf{H}\hat{\mathbf{u}} \tag{37}$$

Substituting Equation (37) into (35), we have

$$\mathbf{UV}^{-1}\mathbf{H}\hat{\mathbf{u}} - \mathbf{H}\hat{\mathbf{q}} = 0 \tag{38}$$

As aforementioned, the evaluation of the main diagonal terms of matrix $\mathbf{V}$ involves only weak singularities, while the main diagonal terms of matrix $\mathbf{U}$ are strongly singular ones. In order to avoid direct numerical integration of these terms, a uniform potential field, namely $u = 1$, can be employed. In the case of uniform field, Equation (38) becomes

$$\mathbf{UV}^{-1}\mathbf{H}\{\mathbf{1}\} = \mathbf{0} \tag{39}$$

where $\{\mathbf{1}\}$ is a column vector with all elements equal to 1. Therefore, the hyper-singular main diagonal terms of matrix $\mathbf{U}$ can be obtained from the off-diagonal terms by using Equation (39).

For a well-posed problem, either $\tilde{u}$ or $\tilde{q}$ is known at each node on the boundary. However, transformations between $\hat{u}_I$ and $\tilde{u}_I$, $\hat{q}_I$ and $\tilde{q}_I$ is necessary because the MLS interpolants lack the delta function property of the usual BEM shape functions as mentioned in Section 2. For the panels where $\tilde{u}$ is prescribed, $\hat{u}_I$ is related to $\bar{u}_I$ by

$$\hat{u}_I = \sum_{J=1}^{N} R_{IJ}\tilde{u}_J = \sum_{J=1}^{N} R_{IJ}\bar{u}_J \tag{40}$$

and for the panels where $\tilde{q}$ is prescribed, $\hat{q}_I$ is related to $\bar{q}_I$ by

$$\hat{q}_I = \sum_{J=1}^{N} R_{IJ}\tilde{q}_J = \sum_{J=1}^{N} R_{IJ}\bar{q}_J \tag{41}$$

where $R_{IJ} = [\Phi_J(\mathbf{s}^I)]^{-1}$ (see Reference [18]).

Equation (38) can be solved in the same way as the conventional BEM. Then, the unknown vector $\mathbf{x}$ is obtained by Equation (37). As can be seen, the present method is a truly meshless one. No boundary elements are used both for interpolation and integration purposes. The computation cost of the matrices $\mathbf{U}$ and $\mathbf{V}$ is similar to that in the traditional BEM. Although we have an extra matrix and an equation to be calculated and solved, the matrix $\mathbf{H}$ is very sparse and easily obtained.

The computational efficiency of the proposed method in comparison with 3D domain schemes, e.g. FEM or EFG, is similar to that of BEM. Actually, considering a 3D mesh with n^3 nodes, the number of boundary nodes is around n^2, both the operation count and the memory requirements for the buildup of matrix equation (38) are of the order $O(n^4)$. The operation count increases to $O(n^6)$ if we attempt to solve the equation with conventional direct solvers such as Gaussian elimination. Therefore, although the dimensionality of a problem at hand is reduced by one, it is less computationally efficient than domain schemes. However, the proposed method significantly reduces the human-labour cost of introducing geometric meshes in complex-shaped structures, which is the main aim of a new class of computer methods, the so-called *meshless* or *element-free* methods. Moreover, the computational efficiency of the Hybrid BNM can be enhanced dramatically if it is combined with the Fast Multipole techniques [19].

4. SOLUTION FOR POTENTIALS AND FLUXES

4.1. Potentials and potential gradients on the boundary

After solving Equation (38), the unknowns $\hat{\mathbf{q}}$ and $\hat{\mathbf{u}}$ are ready for use to calculate the potential $\tilde{u}$ and normal flux $\tilde{q}$ on the boundary by using Equations (8) and (9), respectively. For evaluating the potential gradients on the boundary, we use the following equation:

$$
\begin{Bmatrix} \tilde{q} \\ \partial\tilde{u}/\partial s_1 \\ \partial\tilde{u}/\partial s_2 \end{Bmatrix} = \begin{bmatrix} n_1 & n_2 & n_3 \\ \partial x_1/\partial s_1 & \partial x_2/\partial s_1 & \partial x_3/\partial s_1 \\ \partial x_1/\partial s_2 & \partial x_2/\partial s_2 & \partial x_3/\partial s_2 \end{bmatrix} \begin{Bmatrix} q_1 \\ q_2 \\ q_3 \end{Bmatrix}
\tag{42}
$$

where n_i, $i = 1, 2, 3$, is the components of the unit outward normal vector to the boundary; q_i are potential gradients; $\partial x_i/\partial s_k$, $k = 1, 2$ can be obtained from Equation (1) and $\partial\tilde{u}/\partial s_k$ are calculated by

$$
\partial\tilde{u}/\partial s_k = \sum_{I=1}^{N} \Phi_{I,k}\hat{u}_I
\tag{43}
$$

in which $\Phi_{I,k}$ is given by Equation (13). By solving Equation (42), we obtain the potential gradients q_i on the boundary.

4.2. Potentials and potential gradients at internal points

The potential u and the flux q at an internal point, P, are evaluated by the traditional boundary integral equations as follows:

$$
\begin{aligned}
u(P) &= \int_{\Gamma} U(Q, P)\tilde{q}(Q)\,\mathrm{d}\Gamma - \int_{\Gamma} \frac{\partial U(Q, P)}{\partial n(Q)}\tilde{u}(Q)\,\mathrm{d}\Gamma \\
&= \sum_{\text{panels}} \int_{\Gamma^p} U(Q, P)\tilde{q}(Q)\,\mathrm{d}\Gamma - \sum_{\text{panels}} \int_{\Gamma^p} \frac{\partial U(Q, P)}{\partial n(Q)}\tilde{u}(Q)\,\mathrm{d}\Gamma
\end{aligned}
\tag{44}
$$

$$
\begin{aligned}
q_i(P) &= \int_{\Gamma} U(Q, P)\tilde{q}(Q)\,\mathrm{d}\Gamma - \int_{\Gamma} \frac{\partial U(Q, P)}{\partial n(Q)}\tilde{u}(Q)\,\mathrm{d}\Gamma \\
&= \sum_{\text{panels}} \int_{\Gamma^p} \frac{\partial U(Q, P)}{\partial x_i(P)}\tilde{q}(Q)\,\mathrm{d}\Gamma - \sum_{\text{panels}} \int_{\Gamma^p} \frac{\partial^2 U(Q, P)}{\partial x_i(P)\partial n(Q)}\tilde{u}(Q)\,\mathrm{d}\Gamma
\end{aligned}
\tag{45}
$$

where $U(Q, P)$ is the fundamental solution with Q and P being the field point and source point, respectively. '*panels*' denotes the number of the panels which compose the whole boundary. Since every panel is represented by a unit square in parametric space in Equation (1), the integrations on each panel in Equations (44) and (45) can be performed easily. Here, we develop an adaptive scheme to compute these integrals on a panel. In this scheme, we divide the unit square into four equal quarters at first, (see Figure 3), then for each quarter, we calculate the diagonal length, l, and the distance between the evaluation point and the centre
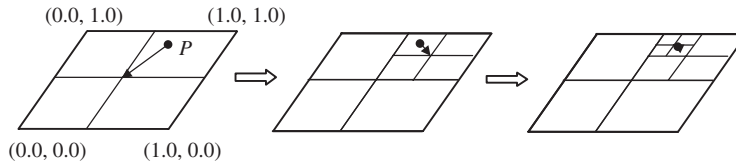
Figure 3. Subdividing of a panel in parametric space corresponding to an evaluation point P.

of the quarter, d, in the real world-co-ordinate system. If l is smaller than d, this quarter is taken as a regular integration patch, or it is further divided into four sub-quarters, and the procedure goes on, until all patches become regular. Finally, using Gaussian quadrature for all patches, we can evaluate the integrals in Equations (44) and (45) very accurately even when the evaluation point is very close to the boundary. It should be pointed out that the patches are not like the elaborately constructed elements in the BEM and FEM. They change for different evaluation points and are very easily to compute, and just used for results recovery. So using these patches does not affect the fact that the hybrid boundary node method is a truly meshless method.

5. ILLUSTRATIVE NUMERICAL RESULTS

The current method has been tested thoroughly for three types of 3D geometrical objects: a sphere, a cube and an elbow pipe. To compare the current method with the BNM, the former two models are taken from Reference [20]. And the last one, a more geometrically complicated one, is added to show the advantage of the truly meshless nature of the present method. In order to assess the accuracy of the present method, the following three analytical fields are used as the exact solutions of the above models:

(i) *Linear solution*

$$u = x + y + z \tag{46}$$

(ii) *Quadratic solution*

$$u = -2x^2 + y^2 + z^2 \tag{47}$$

(iii) *Cubic solution*

$$u = x^3 + y^3 + z^3 - 3yx^2 - 3xz^2 - 3zy^2 \tag{48}$$

In all cases, Laplace's equation $\nabla^2 u = 0$ is solved, together with appropriately prescribed boundary conditions corresponding to the above analytical solutions.

For the purpose of error estimation and convergence study, a 'global' L_2 norm error, normalized by $|u|_{\max}$ is defined as follows [9, 19]:

$$e = \frac{1}{|u|_{\max}} \sqrt{\frac{1}{N} \sum_{i=1}^{N} (u_i^{(e)} - u_i^{(n)})^2} \tag{49}$$

where $|u|_{max}$ is the maximum value of u over N sample points, superscripts (e) and (n) refer to the exact and numerical solutions, respectively.

In all computations, unless indicated otherwise, the support size of the weight function, $\hat{d}_I$ in Equation (15), is taken to be $10.0h$, with h being the minimum distance between the neighbouring points, and the parameter c_I is taken to be such that $\hat{d}_I/c_I$ is constant and equal to 5.0. The size of the local domain (radius r_J) for each node is taken as a free parameter whose value is to be optimized with the highest accuracy, and the parameter c_J in Equation (25) is taken to be such that r_J/c_J is constant and equal to 0.1. To carry out the integrations in Equation (34), each of these local surfaces Γ_s are mapped into a unit circle in the parametric space. This unit circle is further divided into 8 patches, 2 segments in radial direction and 4 segments in circumferential direction. In each patch, 3×3 G points are used for integration.

5.1. Dirichlet problem on a sphere

The example solved here is a potential problem, governed by Laplace's equation, for a sphere of radius 2 unit, centred at the origin. The usual spherical polar co-ordinates θ and ϕ are used. On the surface, 118 uniformly spaced nodes are used. In this example, the linear, quadratic and cubic fields are tested. In each case, the Dirichlet boundary conditions corresponding to the exact solutions have been imposed on the surface of the sphere. The relative errors (Equation (49)) of u and its y derivative inside the sphere, denoted by DM-u and DM-q in the figures, are evaluated over 11 sample points uniformly distributed from $(0, 0, 0)$ to $(0, 1.99, 0)$. The relative errors of u and q ($\equiv \partial u/\partial n$) on the surface, denoted by SF-u and SF-q in the figures, are evaluated over 21 sample points uniformly distributed along the equator of the sphere ($0 \leqslant \theta \leqslant 2\pi$). Results for various values of the sub-domain radius, r_J, are shown in Figure 4. From Figure 4, it is found that the optimal value of r_J is $0.75h$ (where h is the minimum distance of the node $\mathbf{s}_J$ to its neighbouring nodal points). Figure 5 shows the numerical results, together with their analytical solutions, of u and its y derivative along the radius from $(0, 0, 0)$ to $(0, 1.99, 0)$. In the present implementation of the Hybrid BNM, it is appealing that high accuracy can be achieved. By using Equations (44) and (45) to compute the potential and the flux at internal points, the results are not sensitive to the proximity of the interior points to the boundary. This observation is different from that of the results obtained by the Hybrid BNM in 2D case [10] and by other hybrid boundary element methods [16].

To study the convergence of the present method, the cubic field has been tested on three regular node arrangements: (a) 118 nodes, (b) 277 nodes and (c) 492 nodes. Figure 6 shows the convergence of the potential and its y derivative inside the sphere. It can be seen that the present Hybrid BNM has high rates of convergence.

5.2. Dirichlet and mixed problems on a cube

The case of the field for a $2 \times 2 \times 2$ cubic domain governed by Laplace's equation is presented as the second example. The cube faces are $x = \pm 1$, $y = \pm 1$ and $z = \pm 1$, respectively. The cubic polynomial, Equation (48), is considered as the exact solution. A Dirichlet problem is solved for which the essential boundary conditions are imposed on all faces corresponding to the exact solution, and a mixed problem for which the essential boundary condition is imposed on faces $z = \pm 1$, the natural boundary condition is prescribed on faces $x = \pm 1$ and $y = \pm 1$. 10×10 nodes on each face are used.
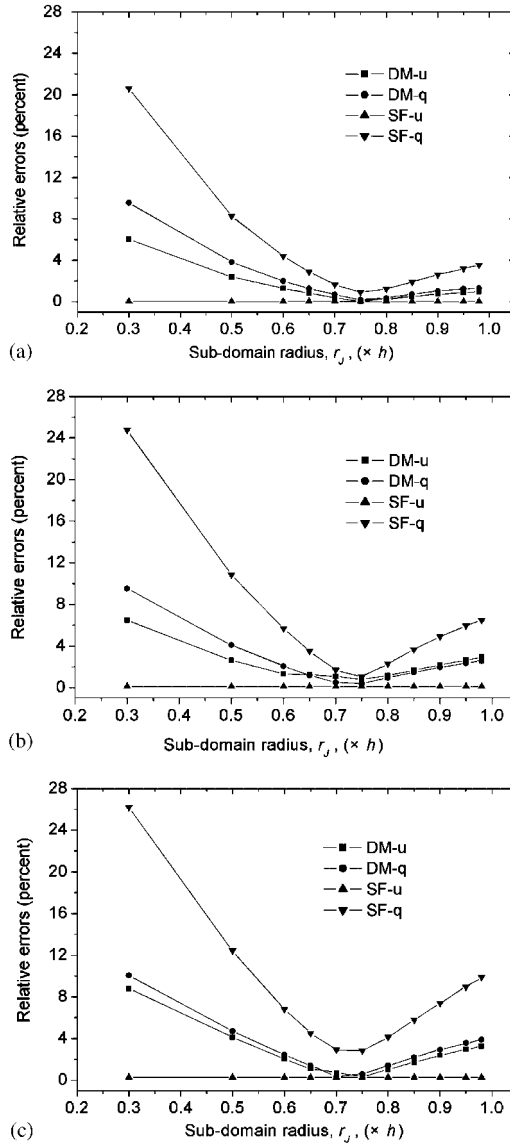
Figure 4. Relative errors of the Dirichlet problem on a sphere for various sub-domain radius, r_J: (a) for the linear field; (b) for the quadratic field; and (c) for the cubic field.

The relative errors of u and its x derivative inside the cube, denoted by DM-u and DM-q in the figures, are evaluated by Equation (49) over 11 sample points uniformly distributed from $(0, 0, 0)$ to $(0.99, 0, 0)$. Results for various values of r_J for the Dirichlet and mixed problems are shown in Figure 7. It is seen that the optimal value of r_J is $0.8h$.

Figure 8 shows the numerical result and the exact value of the z derivative of potential along the diagonal of the face $x = 1$ when different numbers of nodes are used. We observe
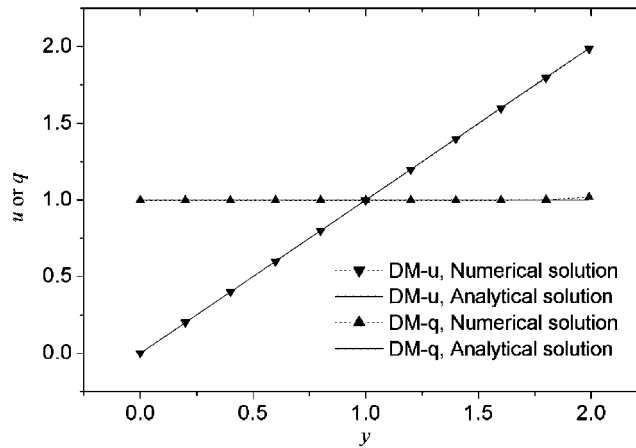
Figure 5. Potential and its y derivative along the radius of the sphere (from $(0, 0, 0)$ to $(0, 1.99, 0)$).
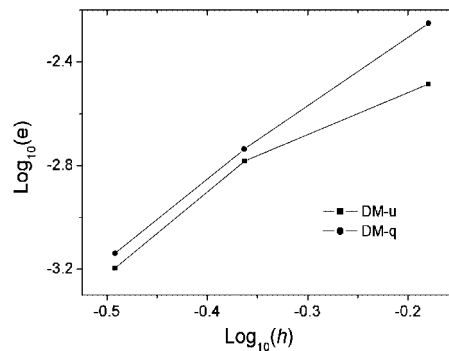
Figure 6. Relative errors and convergence rates for Dirichlet problem on a sphere.

that errors occur mainly at and near the corners. When the number of nodes increases, the errors decrease. Anyway, this remains a subject of the further studies.

5.3. Dirichlet problem on an elbow pipe

In order to show the advantages of the truly meshless nature of the Hybrid BNM, a more complicated geometry is also tested. The geometry and its main sizes are shown in Figure 9. Three cases have been solved for which Dirichlet boundary conditions corresponding to the linear exact solution (Equation (46)), the quadratic exact solution (Equation (47)) and the cubic exact solution (Equation (48)), are imposed on all faces of the elbow pipe, respectively. In all cases, 1560 nodes are used. The relative errors of u and x derivative inside the domain are evaluated on 11 sample points uniformly spaced on an internal line segment from $(0, 7.5, 0)$ to $(5, 7.5, 0)$. Figure 10 shows the relative errors for various values of sub-domain radius r_J. In Figure 10, we find that the optimal value of r_J is $0.8h$. Numerical results for q along
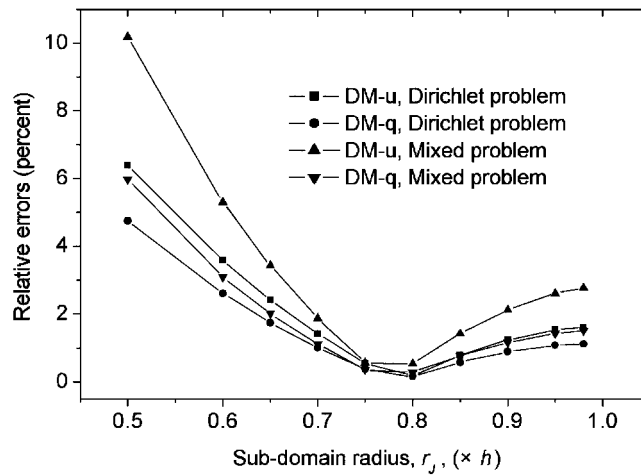
Figure 7. Relative errors of the Dirichlet and the mixed problems on a cube for various sub-domain radius, r_J.
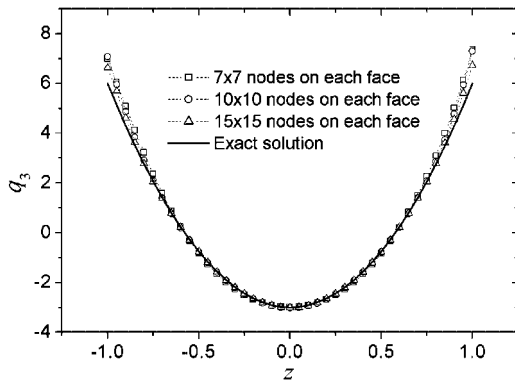

Figure 8. Results of potential gradient q_3 ($\equiv \partial u / \partial z$) along the diagonal of the face $x = 1$ using different node arrangements.
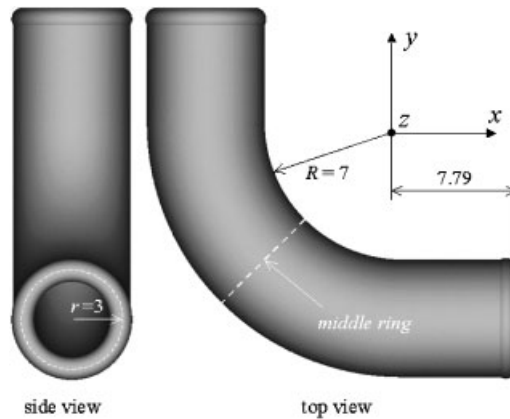

Figure 9. The elbow pipe and its main sizes.

the middle ring (see Figure 9) with $r_J = 0.8h$, together with the exact solution, are shown in Figure 11. The numerical results are in agreement with the exact solutions. It should be pointed out here that the preparation of the input data for this problem is rather simple. We need to define only 8 panels on the surface of the elbow pipe, and do not need any boundary elements. The Hybrid BNM is flexible and convenient, and could be an important step toward complete analysis automation.
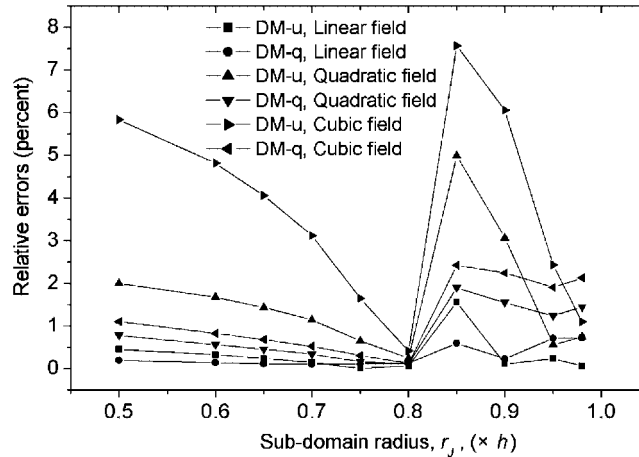
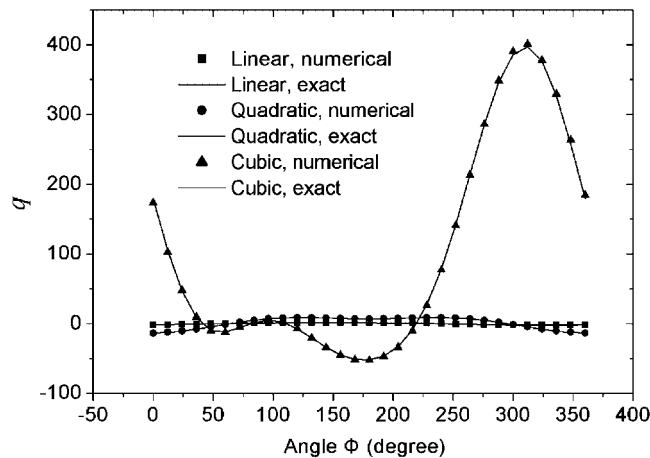Figure 10. Relative errors of the Dirichlet problem on the elbow pipe for various sub-domain radius, r_J.

Figure 11. Normal flux, q, along the middle ring of the elbow pipe.

6. CONCLUSIONS

The hybrid boundary node method has been extended to solve potential problems in three dimensions, and a general scheme of the MLS interpolation on a generic surface has been developed in this paper. The Hybrid BNM is based on a hybrid model that involves three types of independent variables, i.e. potentials and normal fluxes on the boundary and potentials inside the domain. The domain variables are interpolated by the classical fundamental solutions with the source points located on the boundary; and the boundary variables are approximated by the MLS approximation. The advantages of the present method, when compared with other

numerical methods, are as follows:

- Compared with the MLBIE and MLPG, the Hybrid BNM has the well-known dimensionality advantage of the BEM, e.g. for a 3D object, the nodal discretization is restricted only to the 2D bounding surface of the body, and no internal nodes are needed.
- Compared with the conventional BEM, the Hybrid BNM is a meshless method, which requires only a nodal data structure on the boundary, and hence simplifies the work of preparing the input data considerably. To analyse a structure, one needs to define only the panels which make up the boundary of the structure, no boundary elements have to be constructed.
- Compared with the BNM, the Hybrid BNM is a truly meshless method. Absolutely no cells are needed either for interpolation or integration purposes. All integrals can be easily evaluated over regular shaped sub-domains (in general, semi-sphere in the 3D problem) and their boundaries.

The Hybrid BNM has been verified through some numerical examples with known analytical solutions. The appropriate size of the sub-domain radius has been investigated through computations for different geometries, boundary condition types and known analytical fields. It was observed that the optimal values of the sub-domain radius were very close to each other in all cases, and were between $0.75h$ and $0.8h$.

Numerical results have demonstrated the accuracy and convergence of the present method. The solution is accurate for the potentials and fluxes on the boundary and inside the domain. High rates of convergence have been achieved. The serious 'boundary layer effect' in the Hybrid BNM has been circumvented by an adaptive face integration scheme.

By coupling with the Fast Multipole Method, the Hybrid BNM may be able to solve large complicated structures, such as nanotube based composites. This is planned in the near future.

REFERENCES

1. Nayroles B, Touzot G, Villon P. Generalizing the finite element method: diffuse approximation and diffuse element. *Computational Mechanics* 1992; **10**:307–318.
2. Belytchko T, Lu YY, Gu L. Element free Galerkin methods. *International Journal for Numerical Methods in Engineering* 1994; **37**:229–256.
3. Belytchko T, Krongauz Y, Organ D Fleming M, Krysl P. Meshless methods: an overview and recent developments. *Computer Methods in Applied Mechanics and Engineering* 1996; **139**:3–47.
4. Li G, Aluru NR. Boundary cloud method: a combined scattered point/boundary integral approach for boundary-only analysis. *Computer Methods in Applied Mechanics and Engineering* 2002; **191**:2337–2370.
5. Chen W, Tanaka M. New insights into boundary-only and domain-type RBF method. *International Journal of Nonlinear Science and Numerical Simulation* 2000; **1**(3):145–151.
6. Aluru NR. A reproducing kernel particle method for meshless analysis of microelectromechanical systems. *Computational Mechanics* 1999; **23**:324–338.
7. Zhu T, Zhang J, Atluri SN. A local boundary integral equation (LBIE) method in computation mechanics, and a meshless discretization approach. *Computational Mechanics* 1998; **21**:223–235.
8. Atluri SN, Zhu T. A new meshless local Petrov–Galerkin approach in computational mechanics. *Computational Mechanics* 1998; **22**:117–127.

 9. Mukherjee YX, Mukherjee S. The boundary node method for potential problems. *International Journal for Numerical Methods in Engineering* 1997; **40**:797–815.
10. Zhang JM, Yao ZH, Li H. A hybrid boundary node method. *International Journal for Numerical Methods in Engineering* 2002; **53**:751–763.
11. Zhang JM, Yao ZH. Meshless regular hybrid boundary node method. *Computer Modeling in Engineering and Sciences* 2001; **2**:307–318.
12. Zhang JM, Yao ZH, Tanaka M. The meshless regular hybrid boundary node method for 2D linear elasticity. *Engineering Analysis with Boundary Elements* 2003; **27**:259–268.
13. Zhang JM, Yao ZH. Analysis of 2D thin structures by the meshless regular hybrid boundary node method. *Acta Mechanica Sinica* 2002; **15**:36–44.
14. Schnack E. A hybrid BEM model. *International Journal for Numerical Methods in Engineering* 1987; **24**:1015–1025.
15. Dumount NA. The hybrid boundary element method. *Proceedings of the 9th International Conference on BEM*, Stuttgart. Computational Mechanics Publications, Springer: Southampton, Berlin, 1987.
16. DeFigueredo TGB, Brebbia CA. A new hybrid displacement variational formulation of BEM for elastostatics. In *Advances in Boundary Elements*, Brebbia CA, Conner JJ (eds). Computational Mechanics Publications: Southampton, vol. 1, 1989; 47–57.
17. Zhu T. A new meshless regular local boundary integral equation (MRLBIE) approach. *International Journal for Numerical Methods in Engineering* 1999; **46**:1237–1252.
18. Atluri SN, Kim HG, Cho JY. A critical assessment of the truly Meshless Local Petrov–Galerkin (MLPG), and Local Boundary Integral Equation (LBIE) methods. *Computational Mechanics* 1999; **24**:348–372.
19. Nishida T, Hayami K. Application of the fast multipole method to the 3D BEM analysis of electron guns. In *Boundary Elements*, vol. XIX, Marchettia M, Brebbia CA, Aliabadi MH (eds). Computational Mechanics Publications: Southampton, U.K., 1997; 613–622.
20. Chati MK, Mukherjee S. The boundary node method for three-dimensional problems in potential theory. *International Journal for Numerical Methods in Engineering* 2000; **47**:1523–1547.